GEOPHYSICAL RESEARCH LETTERS, VOL. 28, NO. 14, PAGES 2727-2730, JULY 15, 2001

Estimation of rupture propagation direction and strong motion generation area from azimuth and distance dependence of source amplitude spectra

Hiroe Miyake, Tomotaka Iwata, and Kojiro Irikura

Disaster Prevention Research Institute, Kyoto University, Kyoto, Japan

Abstract. Strong motion generation areas which reproduce ground motions in 0.2 to 10Hz were estimated using the empirical Green's function method. This strong motion generation area was somewhat smaller than the total rupture area, and coincident with the area of asperities derived from heterogeneous slip distributions estimated by waveform inversions using lower frequencies (<1Hz). We confirmed that the azimuth and distance dependence of observed source amplitude spectra in the near-source area, i.e. rupture directivity effects, were controlled by rupture propagation style and size of the strong motion generation area. We found that the source displacement spectra at stations in forward rupture propagation directions had higher corner frequencies and steeper high-frequency decays, compared with stations in sideways directions. Stations in backward directions had opposite tendencies. Different relationships between size and average corner frequencies of the strong motion generation area were proposed for unilateral and bilateral ruptures with radial propagation.

Introduction

Rupture directivity effects on amplitudes and durations of far-field seismic waves and their azimuthal variations have been widely discussed. It is also important to quantify the rupture directivity effects in the near-source areas for studying rupture processes and strong ground motions [e.g. *Boore and Joyner*, 1978; *Somerville et al.*, 1997]. Techniques such as source time function deconvolution using empirical Green's functions [e.g. *Mueller*, 1985; *Mori*, 1996] have been applied to extract the rupture directivity effects and source processes.

In this paper, we estimate the strong motion generation area by fitting observed to simulated ground motions using the empirical Green's function method. Then, we show the rupture directivity effects in the near-source area are strongly influenced by rupture propagation style and size of the strong motion generation area. Especially, we focus on not only variations of corner frequencies but also those of high-frequency decays of apparent source displacement spectra depending on azimuth and distance from source to site, by assuming a finite extended fault plane which explains well the observed source amplitude spectra.

Estimation of strong motion generation area

We examined the source model of eight inland crustal earthquakes (M_{JMA}4.9~7.2) which occurred in Japan from 1995 to 1999 (Fig. 1) using near-source strong ground motions. Strong ground motion records were provided by K-NET [*Kinoshita*, 1998] and CEORKA at more than 20 stations located less than 50km from the epicenters. The empirical Green's functions were chosen from their aftershocks (M_{JMA}3.3~4.7) whose focal mechanisms and hypocentral distances were similar to their respective mainshocks. Source processes of some mainshocks have already been estimated by waveform inversions in the low frequency range (<1Hz) [e.g. *Ide*, 1999; *Sekiguchi et al.*, 2000; *Horikawa*, 2001].

We define the 'strong motion generation area' as the characteristic area with large and uniform slip velocity in the total rupture area, and which reproduces the near-source strong ground motions in the frequency range 0.2 to 10Hz. The lower limit of the frequency range comes from the noise level of the aftershock records. In order to estimate the strong motion generation area for the target earthquakes, we simulated acceleration, velocity, and displacement waveforms at four stations surrounding the source areas using the empirical Green's function method [*Irikura*, 1986; *Kamae and Irikura*, 1998]. The strong motion generation area is assumed to be homogeneous rectangular fault plane in the total rupture area, where rupture propagates radially from the hypocenter with the speed of 90% of the *S*-wave velocity, and the shape of the slip velocity function is adopted to be the Kostrov type. Parameters, which are length, width, rupture starting point, and rise-time of the strong motion generation area, were estimated to minimize the summation of the residuals of the displacement waveform fitting and those of the acceleration

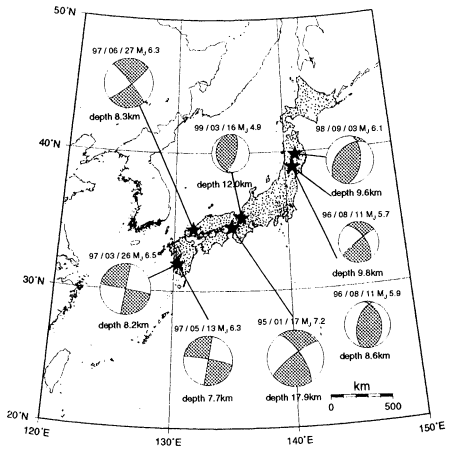

Figure 1. Epicentral locations and focal mechanisms used in this study. Focal mechanisms were determined by moment tensor inversion using broadband seismic waveforms. Black dots indicate observed stations of K-NET and CEORKA.

Paper number 2000GL011669.
0094-8276/01/2000GL011669$05.00

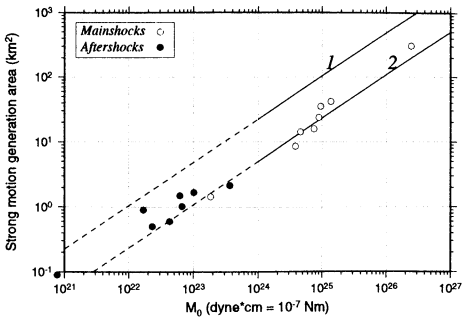

Figure 2. Scaling between strong motion generation area vs. seismic moment. The lines indicated by 1 and 2 correspond to the rupture area and combined area of asperities, respectively, as a function of seismic moment [*Somerville et al.*, 1999]. The area size of the 1995 Hyogo-ken Nanbu earthquake is from *Kamae and Irikura* [1998].

envelope fitting, by the Genetic Algorithm method or forward modeling. The synthetic waveforms for the best parameters fit the observations in the near-source area well [e.g. *Miyake et al.*, 1999]. The style of rupture propagation direction and the strong motion generation area agreed with the rupture processes obtained by the waveform inversions in the low frequency range (<1Hz).

The relationship between size of the strong motion generation area and seismic moment is shown in Fig. 2. This seismic moment was obtained from a moment tensor solution using broadband waveforms [e.g. *Fukuyama et al.*, 1998]. We found that the strong motion generation area was proportional to $M_0^{2/3}$, showing the self-similar scaling relation and coincident with the combined areas of asperities [*Somerville et al.*, 1999] derived from heterogeneous spatial slip distributions estimated by waveform inversions using lower frequencies (<1Hz). This means that the effective area for strong ground motions is small compared to the total rupture area obtained by the waveform inversions.

Rupture directivity effects in observed source amplitude spectra

Based on the above estimation, we classified observed stations into the forward, sideways, and backward directions of the rupture propagation (Fig. 3) for each target earthquake. After taking a 30 seconds time window including the *S*-wave part for every component, we applied the multitaper spectral method [e.g. *Park et al.*, 1987] whose taper produces low spectral leakage. We calculated the observed amplitude spectra as a vector summation of the 3 component amplitude spectra. In order to extract apparent observed source amplitude spectra without the effects of site amplification, we took observed amplitude spectral ratios of the mainshock to its aftershock for each station. We also corrected for the effects of propagation path such as geometrical spreading and Q value. The shape of the observed amplitude spectral ratios at frequencies less than the aftershock corner frequency can be regarded as the source amplitude spectral shape of the mainshock itself. The frequency range used in this spectral analysis was around 0.2~10Hz.

The left trace in Fig. 4 shows typical observed amplitude spectral ratios recorded at several stations surrounding the source areas. When the rupture propagated unilaterally with radial propagation from the rupture starting point, forward, sideways, and backward directivity effects were clearly found in the observed spectral ratios. Source displacement spectra of the mainshock at stations in the forward directions had higher corner frequencies and steeper high-frequency decays compared with stations in the sideways directions. The tendencies at stations in the backward directions were opposite to those in the forward directions. In case of the bilateral rupture event, forward directivity effects were observed near the rupture ends. When the rupture propagated predominantly in an upward direction, forward directivity effects were observed only in the epicentral area. This azimuth and distance dependence of source amplitude spectral shape is considered to the feature of the rupture directivity effects in the near-source area. The difference in rupture directivity effects between the strike-slip and dip-slip events was not so significant from the observed source amplitude spectra.

According to *Somerville et al.* [1997], lower frequency level of source amplitude spectra on strike-normal component is found to be larger than on strike-parallel component, because the difference of the radiation pattern effects appeared in the rupture directivity effects. In this analysis, we discussed source amplitude spectra as sum of the 3 components, then the differences of source amplitude spectra between strike-normal and strike-parallel component is considered to smooth out.

Numerical simulation using the stochastic Green's function method

In order to examine the spatial variations of the rupture directivity effects on the observed source amplitude spectra, we performed numerical simulation using the stochastic Green's function method [*Kamae et al.*, 1991]. So far, most numerical simulations of the rupture directivity effects are applied using a line source multiplied by the directivity factor, $D=1/(1-(Vr/Vs\cos\theta))$ [e.g. *Boore and Joyner*, 1989], where Vr, Vs, and θ are rupture propagating velocity, *S*-wave velocity, and incident angle from the rupture propagation direction, respectively. Here, we assumed a finite extended fault plane for the target earthquake, expressed as a summation of subevents with small fault planes with rupture propagating smoothly and radially from the hypocenter. The seismic wave from each subevent was calculated

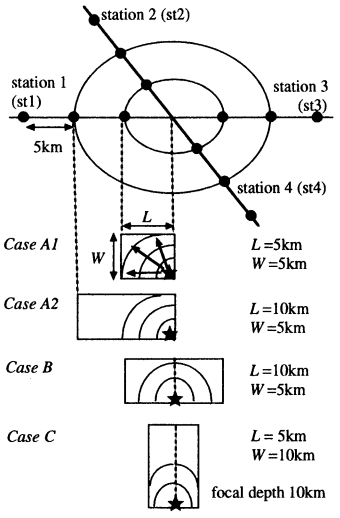

Figure 3. Schematic illustrations of the source models for different rupture propagation styles. Dots and stars indicate stations and rupture starting points, respectively.

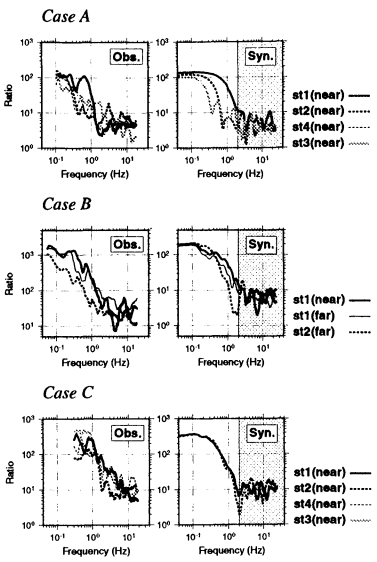

Figure 4. Classification of the rupture propagation style into cases A, B, and C. The Left trace shows the observed amplitude spectral ratios of the mainshock to the aftershock for each rupture style (A: 1997 Kagoshima-ken Hokuseibu earthquake (1997.3.26), B: 1995 Hyogo-ken Nanbu earthquake (1995.1.17), and C: 1997 Yamaguchi-ken Hokubu earthquake (1997.6.27)). Epicentral distance for each station is shown in parenthesis, where near and far means 15km and 30km from the epicenters. The right trace shows source spectral ratios for different rupture styles from the numerical simulations using the stochastic Green's function method. The shadow means higher frequency zone than the corner frequency of the subevent.

using the stochastic simulations produced by *Boore* [1983] following the omega-squared source model [*Brune*, 1970]. This technique was proposed by *Kamae et al.* [1991], and is called the stochastic Green's function method.

As shown in Fig. 3, we assumed the source models for the cases A1, A2, B, and C and divided the near-source area into four

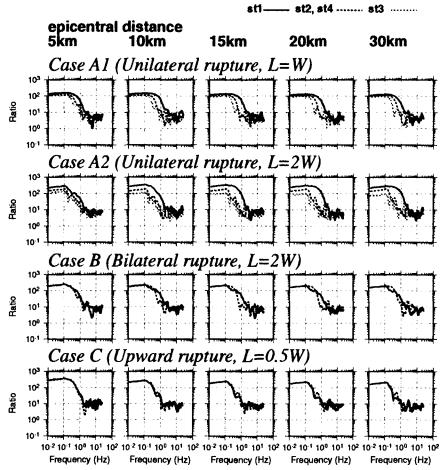

Figure 5. The azimuthal and epicentral distance variations of the source spectral ratios obtained from the numerical simulation. Each subfault size is 1km length by 1km width. Strike=270°, dip=90°, Vs=3.1km/s, and Vr=2.8km/s were fixed for each rupture style shown in Fig. 3.

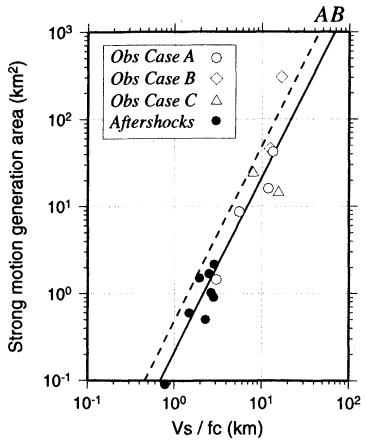

Figure 6. Scaling between size vs. average corner frequency of the strong motion generation area. The lines indicated by A and B show the relationship for unilateral (case A) and bilateral (case B) rupture proposed from our numerical simulation, respectively.

quadrants, with assigned stations 1 to 4. The spectral ratios of the synthetic to the element waveform (the stochastic Green's function) were calculated at intervals of 5km from the epicenter (Fig. 5) with an average radiation pattern factor. We confirmed that the spatial variations of the spectral shape observed in the synthetics were observed in our data. Especially, the variation of spectral decays is simulated successfully by taking into account the effect of incident angle variation from each subfault to the site on the finite fault. Azimuthal variations of corner frequencies for the finite extended fault in unilateral rupture tends to be weaker than $fc=VrD/\pi L$, where fc is corner frequency and L is the length of the fault. This tendency is also considered to be the effect of the incident angle variation. Distance dependence of the source amplitude spectra obtained by the numerical simulation is stronger than that shown in observation. This suggests that the real fault plane isn't so uniform as that assumed in the numerical simulation.

Estimation of rupture propagation direction effects

From azimuth and distance dependence of the source amplitude spectra, the rupture propagation direction and styles was classified into those shown in Fig. 4. That is, A: unilateral rupture, B: bilateral rupture, and C: upward rupture, with radial propagation. Both observation and numerical simulation supported this classification of the source amplitude spectra. If forward, sideways, and backward directivity effects are clearly found in the source amplitude spectra, unilateral rupture propagation is appropriate (case A). If forward directivity effects are observed near the rupture ends, bilateral rupture will be considered (case B). If forward directivity effects are observed only in the near-source region, the rupture propagates predominantly in an upward direction (case C).

Relationship between size and average corner frequency of strong motion generation area

We examined the relationship between size and average corner frequency of the strong motion generation area. The observed average corner frequencies were calculated by taking into account the rupture directivity effects using the source spectral fitting method [*Miyake et al.*, 1999]. From the numerical

simulations using the stochastic Green's function method, we estimated the following relationships between area and *fc*; $R=0.26Vs/fc$ for case A (unilateral case) and $R=0.39Vs/fc$ for case B (bilateral case). R is the radius of the equivalent area of the strong motion generation area πR^2. The observed relationships fit to those derived by the numerical simulations (Fig. 6). We found that it is appropriate to use different equations for different rupture propagation styles. Comparisons with other relationships $R=0.37Vs/fc$ [*Brune*, 1970, 1971], $R=0.32Vs/fc$ [*Sato and Hirasawa*, 1973], and $R=0.21Vs/fc$ [*Madariaga*, 1976], the estimation of R in case B is found to be similar to the estimation from the Brune's equation.

Conclusions

We clarified that the strong motion generation area obtained here is coincident with the area of asperities derived from heterogeneous spatial slip distributions estimated by waveform inversions using lower frequencies (<1Hz). The azimuth and distance dependence of apparent source amplitude spectra is expressed as a function of the rupture propagation style and size of the strong motion generation area. This phenomenon is attributed to be the rupture directivity effect in the near-source area, where the variation of incident angle from source to site is effective. For the source spectral scaling, it is essential to use spectra not only at one station, but at several stations distributed around the epicenter, because rupture directivity effects may distort spectral shape and give different corner frequencies and high-frequency decays.

Acknowledgements. We deeply appreciate K-NET and CEORKA for providing the strong ground motion data. We would like to thank Keiko Kuge and FREESIA project for giving focal mechanism information, and Faculty of Science, Kyushu University and JMA for providing hypocentral information. The comments provided by two anonymous reviewers and editor are highly acknowledged. We are also grateful to Katsuhiro Kamae for allowing us to use the program of stochastic waveforms, Jorge Aguirre for his helpful support using Genetic Algorithm method, James Mori for improvement of this manuscript. Some figures were drawn by GMT Ver.3.0 [*Wessel and Smith*, 1995]. H.M. was supported by Research Fellowships of the Japan Society for the Promotion of Science for Young Scientists. This work was partially supported by Grants-in-Aide for Scientific Research from the Ministry of Education, Science, Sports and Culture of Japan (No.08248111, 11209201).

References

Boore, D. M., Stochastic simulation of high-frequency ground motions based on seismological models of the radiated spectra, *Bull. Seism. Soc. Am.*, *73*, 1865-1894, 1983.

Boore, D. M. and W. B. Joyner, The influence of rupture incoherence on seismic directivity, *Bull. Seism. Soc. Am.*, *68*, 283-300, 1978.

Boore, D. M. and W. B. Joyner, The effect of directivity on the stress parameter determined from ground motion observations, *Bull. Seism. Soc. Am.*, *79*, 1984-1988, 1989.

Brune, J. N., Tectonic stress and the spectra of seismic shear waves from earthquakes, *J. Geophys. Res.*, *75*, 4997-5009, 1970.

Brune, J. N., Correction, *J. Geophys. Res.*, *76*, 5002, 1971.

Fukuyama, E., M. Ishida, D. S. Dreger, and H. Kawai, Automated seismic moment tensor determination by using on-line broadband seismic waveforms, *Zisin2, 51*, 149-156, 1998 (in Japanese with English abstract).

Horikawa. H., Fault models of the two Kagoshima, Japan, earthquakes, submitted to *Bull. Seism. Soc. Am.*, *91*, 112-127, 2001.

Ide, S., Source process of the 1997 Yamaguchi, Japan, earthquake analyzed in different frequency bands, *Geophys. Res. Lett.*, *26*, 1973-1976, 1999.

Irikura, K., Prediction of strong acceleration motions using empirical Green's function, *Proc. 7th Japan Earthq. Eng. Symp.*, 151-156, 1986.

Kamae, K., K. Irikura, and Y. Fukuchi, Prediction of strong ground motion based on scaling law of earthquake, *Journal of Struct. Constr. Engng, AIJ*, *430*, 1-9, 1991 (in Japanese with English abstract).

Kamae, K. and K. Irikura, Source model of the 1995 Hyogo-ken Nanbu earthquake and simulation of near-source ground motion, *Bull. Seism. Soc. Am.*, *88*, 400-412, 1998.

Kinoshita, S., Kyoshin Net (K-NET), *Seism. Res. Lett.*, *69*, 309-332, 1998.

Madariaga, R., Dynamics of an expanding circular fault, *Bull. Seism. Soc. Am.*, *66*, 639-666, 1976.

Miyake, H., T. Iwata, and K. Irikura, Strong ground motion simulation and source modeling of the Kagoshima-ken Hokuseibu earthquakes of March 26 and May 13, 1997, using empirical Green's function method, *Zisin*, *51*, 431-442, 1999 (in Japanese with English abstract).

Mori, J., Rupture directivity and slip distribution of the M4.3 foreshock to 1992 Joshua Tree earthquake, Southern California, *Bull. Seism. Soc. Am.*, *86*, 805-810, 1996.

Mueller, C. S., Source pulse enhancement by deconvolution of an empirical Green's function, *Geophys. Res. Let. 12*, 33-36, 1985.

Park, J., C. R. Lindberg, and F. L. Vernon III, Multitaper spectral analysis of high-frequency seismograms, *J. Geophys. Res. 92*, 12675-12684, 1987.

Sato, T. and T. Hirasawa, Body wave spectra from propagating shear cracks, *J. Phys. Earth*, *21*, 415-431, 1973.

Sekiguchi, H., K. Irikura, and T. Iwata, Fault geometry at the rupture termination of the 1995 Hyogo-ken Nanbu Earthquake, *Bull. Seism. Soc. Am. 90*, 117-133, 2000.

Somerville, P. G., N. F. Smith, R. W. Graves, and N. A. Abrahamson, Modification of empirical strong ground motion attenuation relations to include the amplitude and duration effects of rupture directivity, *Seism. Res. Lett.*, *68*, 199-222, 1997.

Somerville, P., K. Irikura, R. Graves, S. Sawada, D. Wald, N. Abrahamson, Y. Iwasaki, T. Kagawa, N. Smith, and A. Kowada, Characterizing crustal earthquake slip models for the prediction of strong ground motion, *Seism. Res. Lett., 70*, 59-80, 1999.

Wessel, P. and W. H. F. Smith, New version of the Generic Mapping Tools released, *EOS Trans. Am. Geophys. Union., 76*, 329, 1995.

H. Miyake, T. Iwata, and K. Irikura, Disaster Prevention Research Institute, Kyoto University, Gokasho, Uji, Kyoto 611-0011, Japan. (e-mail: miyake@egmdpri01.dpri.kyoto-u.ac.jp, iwata@egmdpri01.dpri.kyoto-u.ac.jp, irikura@egmdpri01.dpri.kyoto-u.ac.jp)

(Received April 11, 2000; revised January 31, 2001; accepted April 19, 2001)